ARTICLE

ACS chemical biology

Probing Mechanism and Transition State of RNA Refolding

Boris Fürtig[†,§], Philipp Wenter[‡], Stefan Pitsch[‡], and Harald Schwalbe[†,*]

[†]Institute for Organic Chemistry and Chemical Biology, Center for Biomolecular Magnetic Resonance, Johann Wolfgang Goethe-University, Max von Laue-Str. 7, D-60438 Frankfurt am Main, Germany and [‡]Laboratory of Nucleic Acid Chemistry, École Polytechnique Fédérale de Lausanne, EPFL-BCH, 1015 Lausanne, France, [§]Present address: Department of Biochemistry, Max F. Perutz Laboratories, Dr. Bohrgasse 9/5, A-1030 Vienna, Austria.

ABSTRACT Kinetics and the atomic detail of RNA refolding are only poorly understood. It has been proposed that conformations with transient base pairing interaction are populated during RNA refolding, but a detailed description of those states is lacking. By NMR and CD spectroscopy, we examined the refolding of a bistable RNA and the influence of urea, Mg^{2+}, and spermidine on its refolding kinetics. The bistable RNA serves as a model system and exhibits two almost equally stable ground-state conformations. We designed a photolabile caged RNA to selectively stabilize one of the two ground-state conformations and trigger RNA refolding by *in situ* light irradiation in the NMR spectrometer. We can show that the refolding kinetics of the bistable RNA is modulated by urea, Mg^{2+}, and spermidine by different mechanisms. From a statistical analysis based on elementary rate constants, we deduce the required number of base pairs that need to be destabilized during the refolding transition and propose a model for the transition state of the folding reaction.

Many ribonucleic acids (RNAs) can adopt more than a single three-dimensional structure. These alternative structures have very similar stability but show substantially different dynamics and function. Structural transitions between a single or several different metastable RNA states and the final most stable state often constitute the rate-limiting steps on the folding pathway toward a functional RNA fold (*1*). RNA refolding can occur co-transcriptionally and can provide the mechanism for both transcriptional and translational regulation (*2*).

Different from RNA folding from an unfolded polynucleotide chain, RNA refolding consists of three distinct steps: (i) the strand displacement that disrupts stabilizing interactions in the starting state, (ii) formation of a transition state, and (iii) strand association to form the final state (*3, 4*). Depending on the RNA sequence, strand dissociation and association can occur in a concerted or in a sequential manner (*5*).

RNA structures are stabilized by a variety of interactions (*6, 7*) including non-electrostatic interactions (hydrophobic, van-der-Waals, and base pair interactions) (*8*) as well as translational, rotational, vibrational, and configurational entropy. Due to the highly charged nature of the RNA, electrostatic interactions with surrounding solvent and with different ions or other charged molecules in solution are of particular importance. Consequently, divalent ions, especially Mg^{2+}, and also polyamines are important for the stability of a distinct RNA fold (*9*). Interestingly, *in vitro* RNA folding and refolding is most efficient in mixtures of counterions that best approximate physiological conditions (*10*). Counterion condensation reduces the net charge of the RNA by 90% (*11*) and compacts the RNA (*12, 13*). Mg^{2+} plays an important role in the formation and function of many

*Corresponding author, schwalbe@nmr.uni-frankfurt.de.

Received for review January 29, 2010 and accepted June 10, 2010.

Published online June 10, 2010

10.1021/cb100025a

© 2010 American Chemical Society

RNAs (*14–16*) as a result of its high charge density and its high free intracellular concentration (*17, 18*). Polyamines are another important class of RNA counterions (*19*), and their concentration in the cell is very low because they are sequestered by nonspecific interactions within the cell (*20–22*). Depending on the polyamine type and modulated by intracellular signals (*23*), the total intracellular concentration is estimated to be in the millimolar range (ranging from 0.1 to 2 mM in mammalian cells to 7 mM in *Neurospora crassa*) (*24, 25*). The polyamine spermidine is known to accelerate RNA folding (*26*).

In this report, we characterize the influence of Mg^{2+} and spermidine on the refolding kinetics of a 34mer bistable (*27*) RNA. The bistable 34mer RNA (*28–30*) adopts an equilibrium between two conformations A and B (Figure 1) with $\Delta G^{exp}(283\ K) = 0.68$ kcal/mol. The technical prerequisite to study the refolding of conformations A and B by real-time NMR methods is the introduction of a photolabile protecting group at different positions in the nucleotide sequence, by which either one of the two bistable conformations (Figure 1) can be stabilized exclusively. *In situ* deprotection of the photolabile group by laser irradiation and subsequent time-resolved NMR data acquisition allow investigation of the kinetics associated with the structural transition.

Previously, we could show that the transition state in the absence of Mg^{2+} or spermidine retains half of the base pairs formed in the initial state during the refolding process (*28, 29*). This finding suggested a refolding process in which disruption of base pairs toward the transition state has to occur as the initial and rate-determining step, followed by propagation concomitant with the formation of new base pairs present in the final conformational state in the refolding process.

In this report, we characterized the influence of high concentrations of urea and various concentrations of Mg^{2+} and spermidine on the kinetics of the structural transition of a 34-mer bistable RNA. Our studies provide insight to how Mg^{2+} or polyamines can interact with the 34mer RNA and how they influence the kinetics of RNA secondary structure rearrangements. Our data lead us to propose a general model for the refolding of bistable RNAs: a pseudoknot structure is formed as the transition state of RNA refolding that accommodates the maximum number of mutally non-exclusive base pairs to be formed and likely provides the minimum free energy path during RNA refolding.

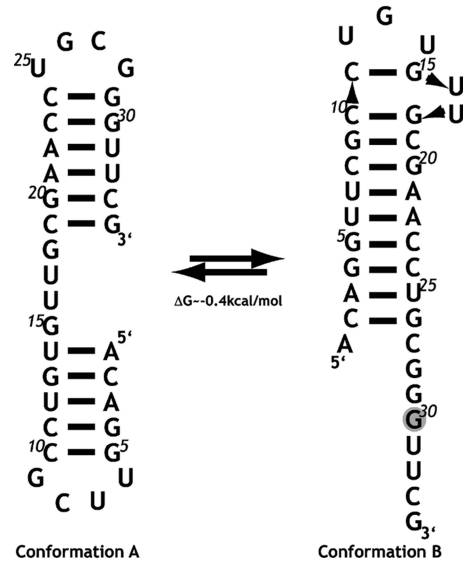

Figure 1. A bistable RNA. Conformation A consists of two hairpin stem-loop secondary structure elements connected by four single-stranded nucleotides. The hairpin stem-loop structure at the 5′-end of the molecule consists of five base pairs capped by an YNMG-tetraloop and at the 3′-end of the molecule of six base pairs capped by an YNMG-tetraloop. In conformation B, there is a single unpaired nucleotide (A1) and a nine-base pair canonical stem that is closed by a sequence of seven nucleotides at the 5′-end, while at the 3′-end there is a single-stranded overhang of eight nucleotides. Introduction of a photolabile NPE group in the nucleobase of guanosine (G30) (shaded in gray) leads to exclusive population of the photoprotected conformation B by destabilizing the C23−G30 base bair in conformation A.

RESULTS AND DISCUSSION

Analysis of Refolding Kinetics by Realtime NMR

Analysis. For realtime NMR investigations, we introduced a photolabile group [1-(2-nitrophenyl)ethyl group] blocking the Watson−Crick side of G30 to selectively destabilize conformation A. The sequence exclusively adopts conformation B (see Figure 1), in which the photolabile nucleotide is part of a single strand. After *in situ* (*31, 32*) photochemical deprotection with a laser pulse of ~1 s, relaxation of conformation B into equilibrium is monitored. The RNA refolding kinetics is slow (see Table 1). After having determined previously the kinetics and thermodynamics of the refolding in the absence of Mg^{2+} or spermidine (*28*), we now characterize their influence on the kinetics of the refolding transition.

TABLE 1. Summary of kinetic rates

	T [K]	$k_{(A\rightarrow B)}$ [s^{-1}]	$k_{(B\rightarrow A)}$ [s^{-1}]	b^a
RNA[b]	288	$3.0 \pm 0.4 \times 10^{-5}$	$8.0 \pm 0.1 \times 10^{-5}$	1
RNA[b]	298	$5.5 \pm 0.9 \times 10^{-4}$	$2.3 \pm 0.6 \times 10^{-4}$	1
RNA[b]	313	$1.3 \pm 0.1 \times 10^{-2}$	$1.7 \pm 0.2 \times 10^{-2}$	1
RNA in 4.5 M urea	283	$5.0 \pm 0.7 \times 10^{-4}$	$2.0 \pm 0.3 \times 10^{-4}$	1
RNA in 4.5 M urea	313	$1.0 \pm 0.2 \times 10^{-2}$	$7.0 \pm 0.1 \times 10^{-3}$	1
RNA in 3×10^{-6} M Mg^{2+}	298	$5.0 \pm 0.7 \times 10^{-4}$	$4.0 \pm 0.6 \times 10^{-4}$	1
RNA in 1×10^{-4} M Mg^{2+}	298	$4.0 \pm 0.5 \times 10^{-4}$	$3.0 \pm 0.1 \times 10^{-4}$	1
RNA in 2×10^{-3} M Mg^{2+}	298	$2.0 \pm 0.5 \times 10^{-4}$	$1.0 \pm 0.3 \times 10^{-4}$	1
RNA in 2×10^{-3} M Mg^{2+}	313	$3.0 \pm 0.3 \times 10^{-2}$	$3.0 \pm 0.3 \times 10^{-2}$	1
RNA in 10^{-2} M Mg^{2+}	298	$3.6 \pm 1.1 \times 10^{-1}$	$1.5 \pm 0.5 \times 10^{-1}$	0.47 ± 0.09
RNA in 2×10^{-4} M SPD	298	$1.8 \pm 0.3 \times 10^{-2}$	$3.1 \pm 0.6 \times 10^{-3}$	0.23 ± 0.1
RNA in 5×10^{-4} M SPD	298	$1.6 \pm 0.2 \times 10^{-1}$	$4.8 \pm 0.6 \times 10^{-2}$	0.39 ± 0.03
RNA in 10^{-3} M SPD	298	$2.6 \pm 0.3 \times 10^{-1}$	$1.7 \pm 0.2 \times 10^{-1}$	0.42 ± 0.02

[a]Stretch factor as discussed in the text. [b]Rates measured for RNA in the absence of cosolvents at an RNA concentration of 0.1 mM are identical to those reported (*28*).

The presence of Mg^{2+} affects the rates of RNA refolding. At concentrations *below* saturation (3 mM Mg^{2+} at an RNA concentration [RNA] = 100 μM and a concentration of monovalent ions [K^+] = 70 mM), the kinetic behavior is not markedly different from the Mg^{2+}-free situation (Table 1) but changes at high Mg^{2+} concentrations. Here, in an initial "burst-like" phase (see Supplementary Figure S1), a fast change is monitored that is followed by a second slower phase leading to deviations from monoexponential refolding kinetics described in eq 2 (see Methods). In principle, the rates can be fitted to biexponential kinetics. Because of the absence of any hint for intermediate formation, however, we analyze the kinetic data using a modified formula that contains an exponential stretch factor to describe the kinetic behavior of the system. As introduced by Kohlrausch (*33*), such stretch factor is used to describe the decay of complex systems from a nonequilibrium state to the equilibrium state. In the context of the folding reaction, complex systems are characterized by their conformational heterogeneity. The smaller the stretch factor b, the larger is the variation of kinetic rates describing the underlying transition. Fit to the formula (see Methods, eqs 3a and 3b) results in the two rate constants k_i for the forward and reverse conformational transition and in the stretch factor b.

In the presence of 10 mM Mg^{2+} ([RNA] = 100 μM), we observe rate constants $k_{(A\rightarrow B)}^{(10\ mM\ Mg^{2+},\ 298\ K)} = 0.36 \pm 0.11\ s^{-1}$ and $k_{(B\rightarrow A)}^{(10\ mM\ Mg^{2+},\ 298\ K)} = 0.15 \pm 0.05\ s^{-1}$ and a stretch factor of $b = 0.47 \pm 0.09$ (Figure 2, panel b). Also spermidine affects the rates of refolding, and the kinetics of the refolding are best described by stretched exponential functions even at low concentrations (Table 1). The kinetics display a very fast phase of the relaxation toward the equilibrium and a second slower phase. For increasing concentrations of spermidine, the individual rates for the forward and backward reaction increase and the stretch factor decreases.

To gain insight into the kind of interactions that lead to significant change in the refolding behavior of the RNA, urea as a denaturant was tested for its effect on the relaxation kinetics. Addition of 4.5 M urea increases the rates of RNA refolding. At 293 K, the equilibrium is already reached after 500 s, whereas only a 10% change of the populations involved in the conformational equilibrium can be observed in the absence of urea (Figure 2, panel a). The rates of RNA refolding in 4.5 M urea range from $k_{(A\rightarrow B)} = 5.0 \times 10^{-4}\ s^{-1}$ and $k_{(B\rightarrow A)} = 2.0 \times 10^{-4}\ s^{-1}$ at 283 K up to $k_{(A\rightarrow B)} = 1.0 \times 10^{-2}\ s^{-1}$ and $k_{(B\rightarrow A)} = 0.7 \times 10^{-2}\ s^{-1}$ at 313 K. The Arrhenius analysis (see Supplementary Figure S2) reveals only a modest temperature dependence that leads to an activation energy $E_{A(A\rightarrow B)}^{(urea)} = 3.2 \pm 0.8$ kcal/mol and $E_{A(B\rightarrow A)}^{(urea)} = 3.8 \pm 0.9$ kcal/mol compared to the 10 times higher value determined in the absence of urea ($E_{A(A\rightarrow B)}^{(free)} = 45 \pm 2$ kcal/mol and $E_{A(A\rightarrow B)}^{(free)} = 40 \pm 1$ kcal/mol). The lower tem-

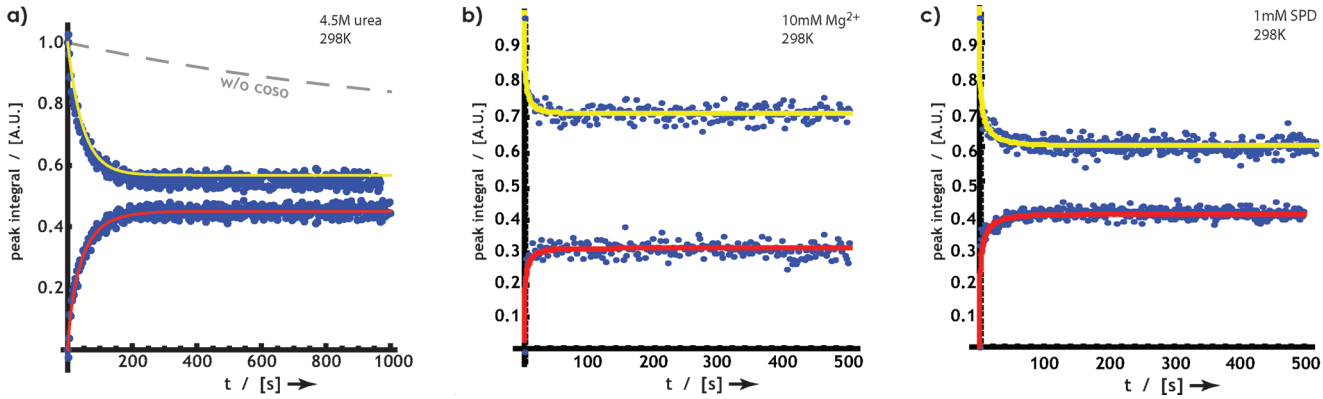

Figure 2. Kinetics of RNA refolding in the presence of cosolvents. a) Kinetic trace in the presence of 4.5 M urea at 293K (blue points), the respective fit to a two-state relaxation process (yellow line), and the theoretical trace (dashed red line) in the absence of cosolvent. b) Kinetic trace recorded in the presence of 10 mM Mg^{2+}. c) Kinetic trace recorded in the presence of 1 mM spermidine (SPD). Experiments shown here were conducted on samples containing 100 μM RNA at 298 K on a 800 MHz NMR spectrometer equipped with a cryogenic probe. Per single experiment two transients were recorded. Blue dots represent experimental data, and solid lines show the fits of the data.

perature dependence leads to significant increase in refolding rates at low temperatures. We conclude that the slow kinetics of RNA refolding is accelerated by Mg^{2+}, spermidine, and high concentrations of urea.

Characterization of Thermal Melting by CD Spectroscopy. CD-spectra recorded for the 34mer RNA at 293 K show the typical strong positive band at 268 nm and two negative bands at 235 and 210 nm for RNA (*34, 35*).

The addition of 3 mM Mg^{2+} (blue line in Supplementary Figure S3a) induces only small changes resulting in less than 5% decrease of the molar ellipticity at 268 and 210 nm. More pronounced changes are monitored when urea is added (red line); the molar ellipticity is reduced by 30% at both wavelengths. A concentration-dependent decrease is also monitored upon addition of spermidine (yellow line).

The melting profiles of the RNA reveal sigmoidal shapes. In the absence of Mg^{2+}, spermidine, or urea, a sharp transition is monitored at $T^{free}_{M(main)} = 355$ K (see Supplementary Figure S3b and S3c), and inspection of the first derivative of the melting profile indicates an additional minor transition at $T^{free}_{M(minor)} = 313$ K (Supplementary Table S1). In the presence of 4.5 M urea, the melting curve is shifted toward lower temperatures; the minor transition, however, remains unaltered. The addition of 3 mM Mg^{2+} increases the stability of the RNA and shifts the transition temperature to $T^{Mg^{2+}}_{M(main)} = 360$ K ($\Delta T^{Mg^{2+}} = +5$ K). Similar effects are observed upon addition of spermidine at higher concentrations ($\Delta T^{SPD/RNA=5:1} = +4$ K) and also affects the minor transition ($\Delta T^{SPD/RNA=5:1}_{M(minor)} = +13$ K).

Characterization of Ground-State Conformations by NMR. The NMR signals of imino protons report on RNA structural dynamics. They provide a characteristic fingerprint for changes in the base pairing pattern of an RNA as each of them is visible only if engaged in a hydrogen-bonding interaction (for example, see Figure 4). Line widths of imino protons are markers for the stability of individual base pairs. The chemical shifts of the imino protons of the 34mer RNA are marginally affected by the addition of 4.5 M urea, and variations of the chemical shift changes along the sequence are not observed (Figure 3). The two most pronounced changes of imino chemical shifts arise from the signals of G26 and U25 (Figure 3a, panel) with $\Delta\delta^{imino} = 134$ Hz and $\Delta\delta^{imino} = 104$ Hz (average $< \Delta\delta^{imino} \geq 62$ Hz), respectively. These two imino protons are involved in the terminal base pairs present in the stem-loop conformation B. Since also the pattern of NOE cross peaks are unchanged upon addition of urea, we conclude that even in the presence of 4.5 M urea, the RNA structure remains unaltered.

Addition of Mg^{2+} leads to small chemical shift changes of almost all imino-proton resonances. At high concentrations of 6 mM Mg^{2+}, the largest shift change is $\Delta\delta^{imino,max} = 74$ Hz. The overall pattern of resonances remains unaltered, indicating the integrity of the RNA structure. Experiments with paramagnetic Mn^{2+} ions lead to similar broadening of all imino signals. We con-

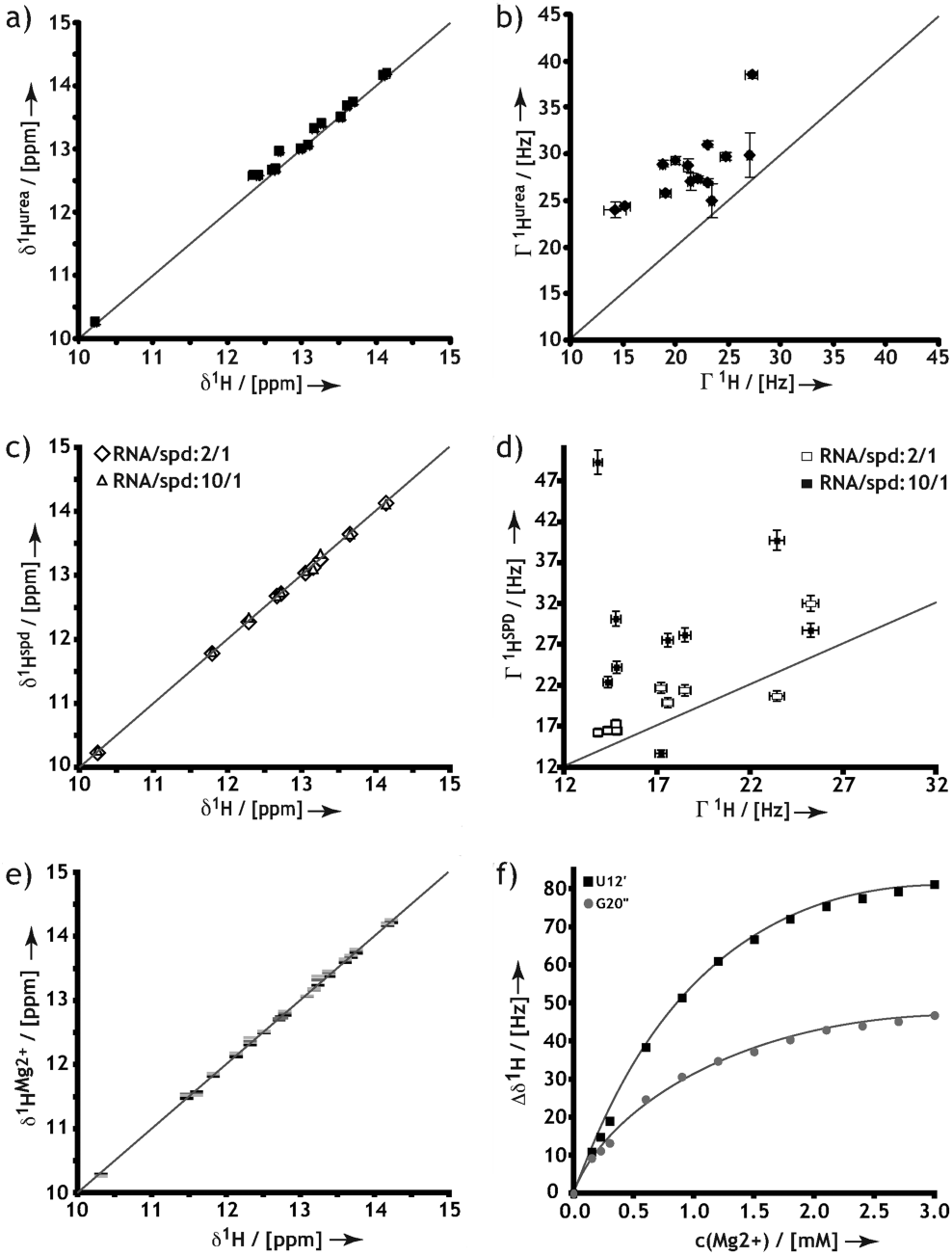

Figure 3. Influence of cosolvents on NMR chemical shifts and line width. Changes of a) chemical shifts and b) linewidths of the imino-resonances upon addition of 4.5 M urea. Changes of c) chemical shifts and d) linewidths upon addition of spermidine in concentrations as indicated in the figure ([RNA] = 100 μM). e) Changes of chemical shifts when adding Mg^{2+} in increasing concentration (increase in Mg^{2+} concentration from 0.15 to 1.2 and 3.0 mM is pictured from black bars to light gray bars). f) Two representative titration curves upon addition of Mg^{2+} for imino resonances of U12 stemming from conformation A (black lines and square symbols) and G20 stemming from conformation B (gray lines and circle symbols).

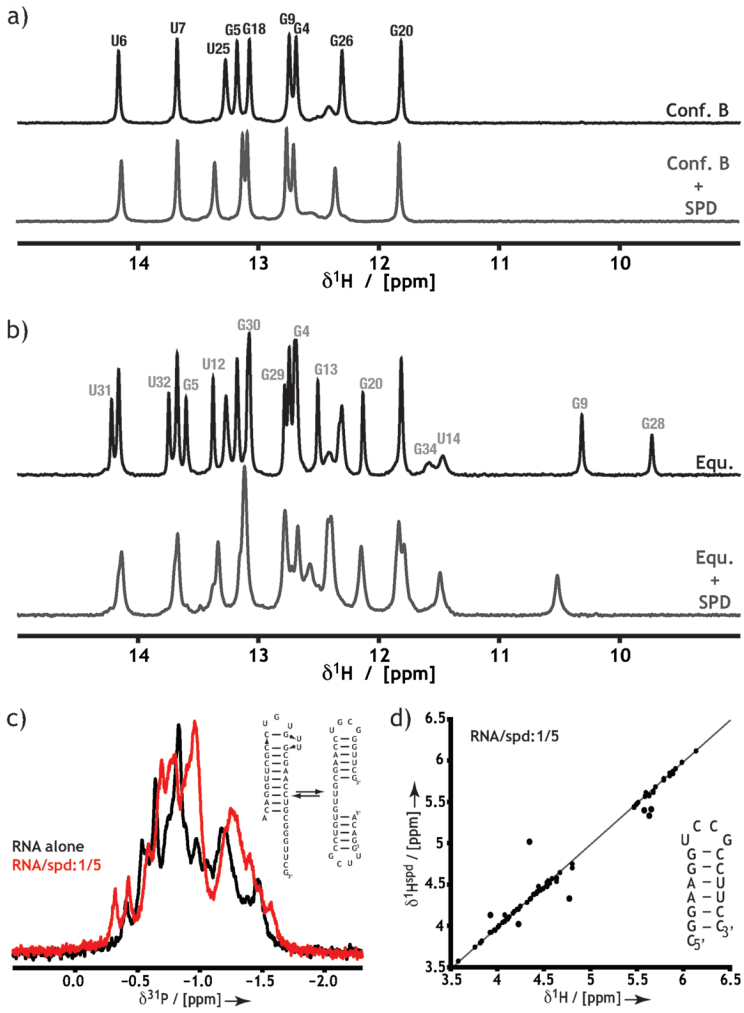

Figure 4. Spermidine-induced changes on properties of the RNA system. Imino-spectral region of the 34mer RNA in the absence (black) and presence (dark gray) of 10 equiv of spermidine. a) Photoprotected sequence stabilizing conformation B under both conditions; b) equilibrium of both conformations A and B under both conditions. The line width is increased by a factor of 10 for the equilibrium case and here the two signals of the noncanonical base pairs for the tetraloops merge. Changes in the sugar−phosphate backbone of RNA molecules upon addition of spermidine as monitored by NMR chemical shift changes. c) 1D ^{31}P spectra of the 34mer RNA in equilibrium of two conformations in absence (black) and presence (red) of spermidine. d) Pronounced changes in chemical shifts of the sugar-backbone atoms upon addition of spermidine to a final ratio of 5:1, as measured for a small 17mer model RNA, representing a structural element as found in the 34mer RNA system.

clude that there are no preferred binding sites for divalent metal ions. Titration of RNA with increasing amounts of Mg^{2+} saturates at $[Mg^{2+}] \approx 3$ mM for both conformations ([RNA] = 100 μM).

Addition of spermidine to the 34mer RNA leads to more complex changes in the NMR spectra. At a 1:1 ratio, small chemical shift changes of imino ^{1}H resonances are observed ($<\Delta\delta^{imino} \geq 40$ Hz). The resonances of the terminal base pairs are affected most. Signals from the two non-canonical base pair interactions in the two YNMG tetra-loops in conformation A collapse into a single signal of double height at a spermidine to RNA ratio of 5:1. The changes in chemical shift follow an apparent saturation curve that levels off at spermidine:RNA ratios higher than 10:1. To further elucidate the effect of spermidine, we monitored chemical shift changes for a reference hairpin that resembles a single stem-loop found in conformation A (see Supplementary Figure S4). The 17mer-hairpin (Figure 4, panel d) adopts a regular A-form helix, in which the nucleotides G2-G7 are base paired with C12−C17 to form a stem structure that is capped by a canonical YNMG-loop (nucleotides U8-G11). Interestingly, upon addition of spermidine, a large number of chemical shift changes can be observed for the sugar moieties. Moreover, we observe two sets of signals for a fraction of resonances upon addition of spermidine. Doubling of peaks is observed for terminal nucleotides at the 5′ and 3′ end of the RNA, in particular for nuclei pointing toward the minor groove of the A-form helix. Spermidine interacts mainly with the phosphodiester backbone of the RNA, since the most pronounced changes in chemical shifts are monitored in the ^{31}P 1D spectrum upon spermidine addition (Figure 4, panel a).

The line widths of the imino-proton signals are sensitive to their chemical exchange with protons of the bulk solvent water. By weakening a particular base pairing interaction, exchange is facilitated leading to an increase in line width (*36*). Large changes of line width were observed in the presence of 4.5 M urea. We could detect an increase in the line width of the RNA imino-proton signals ranging from $\delta\Gamma^{298\ K,4.5\ M\ urea} = 5$ Hz to $\delta\Gamma^{298\ K,4.5\ M\ urea} = 16$ Hz (see Figure 3, panel b), while a reference peak shows only a modest variation of $\delta\Gamma^{298\ K,4.5\ M\ urea} = 0.4$ Hz. This 2-fold increase in line width is significant even when taking the increase in viscosity into account and indicates base pair destabilization by addition of urea.

In the case of spermidine, an increase in line width for the imino resonances is also observed (see plot in Figure 3, panel d and spectrum in Figure 4). Surprisingly, the change in line width is small and in the range of $<\delta\Gamma^{298\ K,\ 30\ h\nu,10/1SPD} \geq 1.6 \pm 1.1$ Hz for the folding in-

competent photoprotected 34mer RNA molecule that adopts only one of the two possible conformations. In contrast, in the equilibrium situation where both folding competent conformations A and B are present, the increase in line width is much more pronounced ($<\delta\Gamma^{298\ K,\ equil.,\ 1:10SPD} \geq 12.5 \pm 6.7$ Hz) and dependent on the concentration of the polyamine ($<\delta\Gamma^{298\ K,\ equil.,\ 1:2SPD} \geq 3.23 \pm 1.1$ Hz).

Previously, we have investigated the kinetics of RNA refolding in the absence of cations or urea and could derive rates and activation energies for this process (*28–30*). Here, we investigate the effect of the physiologically important cations Mg^{2+} and spermidine, which together with urea we refer to as cosolvents, on the thermodynamic stability of a model RNA and on the kinetics of its refolding. We describe the kinetic behavior of interconverting RNA using a general model applying statistical thermodynamics. From the effects observed for imino chemical shifts and linewidths upon addition of cosolvents, we conclude that the bistable RNA does not adopt a single conformation with persistent base pairs possible but rather represents an ensemble of conformations characterized by different numbers of base pairs. The population and distribution of the ensemble of conformations is markedly affected by the nature of the cosolvent, which in turn influences the stabilities as well as the kinetics of refolding of a bistable RNAs.

The ensemble is described by a Boltzmann distribution that relates the relative population of RNA conformers with different numbers of base pairs to the free energy of each conformer. We approximate the free energy of each conformer on the basis of secondary structure prediction models. Then, we assign a forward refolding rate to each conformer based on the experimental finding that the rate-limiting step on the refolding trajectory is the unfolding of secondary structure (*28*). We can then mathematically describe the changes in the concentration of the two conformations A and B involved in RNA refolding by the following formula:

$$\left|\begin{aligned}\frac{dA}{dt} &= \left(\sum_{i=1}^{\max\ bp(A)} -k_i \cdot a_i \cdot A[t]\right) + \left(\sum_{i=1}^{\max\ bp(B)} n_i \cdot b_i \cdot B[t]\right)\\ \frac{dB}{dt} &= \left(\sum_{i=1}^{\max\ bp(A)} k_i \cdot a_i \cdot A[t]\right) + \left(\sum_{i=1}^{\max\ bp(B)} -n_i \cdot b_i \cdot B[t]\right)\end{aligned}\right| \quad (1)$$

where a_i and b_i denote the population of a certain conformer in the ensemble of structures representing folds A and B, respectively, and k_i and n_i the refolding rates according to the number of base pairs that are present in this state.

In the absence of any cosolvent, we obtain a distribution of populations similar to the Boltzmann distribution calculated from the free energies derived from mfold secondary structure predictions. It is noteworthy to mention that although the populations follow an exponential decay with decreasing number of base pairs, the decay is less steep than predicted by the exponential stability dependence. This finding indicates that even in the nonperturbed cosolvent-free state, a considerable population of non-base-paired conformers is present. The Boltzmann distribution based on secondary structure stability prediction assigns only 1.8% and 1.9% of the ensemble of conformations A and B, respectively, to populate open conformations [conformations with $\Delta bp > 0$]), whereas fitting to the experimental kinetics yields a 10 times higher population of open states with 13% and 27%.

In the presence of 4.5 M urea, the kinetics of refolding is markedly affected. At a lower temperature (283 K), the refolding reaction is accelerated by factors up to 30, whereas at high temperature (313 K), the relative effect of urea in increasing the rate constants is considerably smaller. Modeling the reaction kinetics within the frame of the above-described model reveals that the distribution of conformers around the main bistable states A and B changes toward a larger population of open states (Figure 5, panel c). This conclusion is in line with the effect of urea to weaken hydrogen bonds, with the increased NMR line width and the reduction in the thermal stability of the RNA as judged by the CD melting curve. However, even in 4.5 M urea, the structures of the two bistable states remain intact. The strong temperature dependence of the refolding reaction observed in the absence of cosolvent is reduced, consistent with the lower activation energy revealed from the Arrhenius analysis in the presence of 4.5 M urea. The chemical denaturation effect of urea resembles the thermal melting of an RNA.

The presence of Mg^{2+} does not induce major structural changes. We do not find evidence for any high-affinity binding site of Mg^{2+}, a finding not unexpected because both conformations are composed of rather canonical structural elements. Importantly, our investiga-

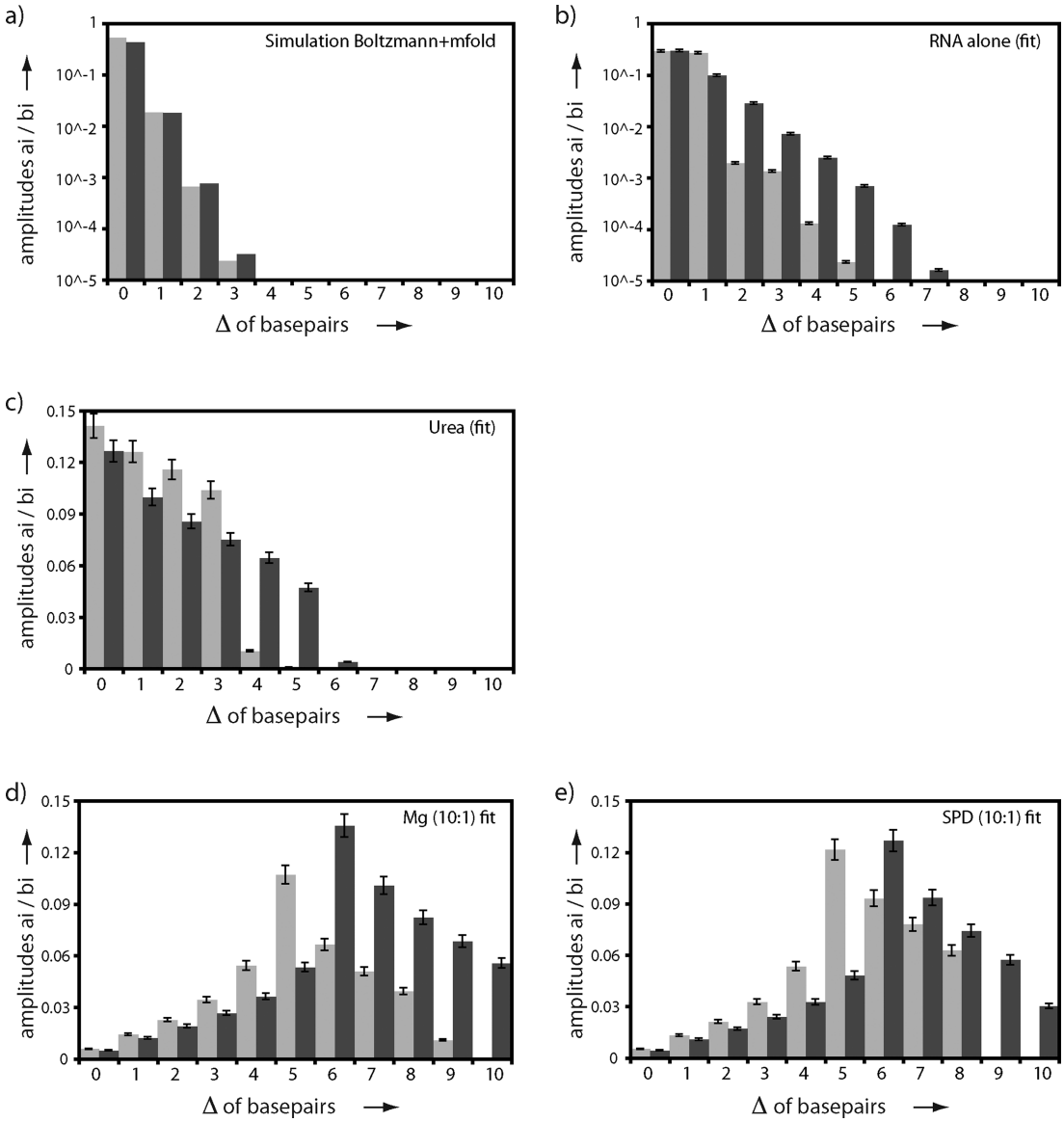

Figure 5. Distribution of amplitudes for the possible members of the confomer ensembles during the refolding process of the 34mer RNA system (dark gray bars represent conformation A and light gray bars represent conformation B) at $T = 298$ K Panels a and b represent the distribution in the RNA in the absence of cosolvent. a) Distribution calculated as a Boltzmann ensemble from simulated energies derived from m-fold; b) actual fit of the data to eq 1. c−e) Results of the best fits of the kinetic traces for the system in 4.5 M urea, 10:1 Mg^{2+}, and 10:1 SPD, respectively, using eq 1.

tions reveal that the kinetics of refolding is dependent on the Mg^{2+} concentration. At low concentrations ($[Mg^{2+}] \approx 3 \times 10^{-6}$ M) below or close to the saturation level ($[Mg^{2+}] = 3$ mM (see Figure 3, panel f)), the kinetic rates in the presence or absence of Mg^{2+} are almost identical, and our observation suggest even a slight decrease in the refolding rates ($k = 5.0 \pm 0.7 \times 10^{-4}$ s^{-1} and $k = 8.0 \pm 0.9 \times 10^{-4}$ s^{-1} at $[Mg^{2+}] = 3 \times 10^{-6}$ M). At high concentrations above saturation, the refolding kinetics is very significantly accelerated by Mg^{2+} and shows no simple exponential behavior anymore. As described above, we fitted the kinetics with a modified for-

malism that introduces a quantitative stretch factor *b*. For low concentrations of Mg^{2+}, this factor adopts values of $b = 1$ and therefore indicate that the ensemble of interconverting conformers is very homogeneous. In contrast, at high concentrations of Mg^{2+}, the kinetics can be described only if the stretch factor is decreased to a value of $b = 0.47$ (see Table 1). In the quantitative description of the system as an ensemble of open and closed conformations, the kinetic measurements at high concentrations of Mg^{2+} translate to a shifted conformational distribution of open states toward a higher population of open states as compared to the RNA only situation. The distribution peaks at $\Delta bp = 6$ and $\Delta bp = 5$ for conformation A and conformation B, respectively (Figure 5, panel d). Taking into account the notion that refolding occurs *via* a transition state with only half of the base pairs formed, these results suggest that Mg^{2+} at such higher concentrations might stabilize open conformations. In line with our findings, previous reports have shown that Mg^{2+} ions exert different effects for different secondary structures. The affinity of Mg^{2+} to folded compact RNA states has been reported to be higher than to extended unfolded RNA states ($K^{folded} = 4.76 \times 10^2\ M^{-1}$; $K^{unfolded} = 2.56 \times 10^2\ M^{-1}$) (*37*). In addition, the binding affinity to a pseudoknot is increased by a factor of ~10 compared to simple hairpins ($K^{pseudoknot} = 1.2 \times 10^3\ M^{-1}$) presumably because the distance between phosphate moieties is very small (*38*). Our kinetic results lead to the conclusion that Mg^{2+} present in concentrations below saturation increases the energetic difference between A and B and the transition state consistent with a slight decrease in refolding kinetics. This observation could also be accounted for by differential stabilization of either one of the two conformations. By contrast, we reason that at Mg^{2+} concentrations beyond the saturation level, the transition state can be stabilized. The hypothesis of transition state stabilization is consistent with the notion that pseudoknots have been reported to have a higher affinity to Mg^{2+} than regular RNA structures.

A yet different effect on the bistable RNA system is observed in the presence of the polycation spermidine (Figure 5, panel e). Apparently, the effects observed for urea and Mg^{2+} *separately* are monitored for SPD *simultaneously*. SPD increases the thermal stability of the ground state as judged by CD-melting curves ($\Delta T = +4$ K at 0.5 mM SPD) as does Mg^{2+}. In addition, it destabilizes secondary structure as judged by static CD spectroscopy. Therefore, the higher temperature stability surprisingly goes along with a reduction of A-form helical content at ambient temperatures. Interestingly, except for the terminal tetraloops, no significant changes can be detected in NMR experiments, suggesting that the base pairing pattern remains essentially intact. The increase in line width of the imino-proton signals of the equilibrium conformations indicates increased dynamics in the individual base pairs. It is captivating to note that the detected base pair dynamics is linked to those systems that can refold, *e.g.*, the bistable RNA depicted in Figure 1. If the refolding capability is suppressed as in the caged 34mer or the 17mer subfragment of the larger RNA, then spermidine does not induce any ground-state dynamics and increased linewidths are not observed (Figure 4, panels a and b).

Even at low concentrations of spermidine, a very significant acceleration of the refolding reaction is observed. The acceleration is concentration-dependent, and the reaction kinetics can qualitatively be described using a stretched exponential function. As noted in Table 1, both rates and stretch factors increase with increasing concentrations of spermidine. Similar to Mg^{2+}, the properties of the system are consistent with a model according to which spermidine induces structural heterogeneities in the two ground-state conformations of the bistable RNA at equilibrium. The induced structural heterogeneities lead to an ensemble of ground-state conformations with different individual refolding kinetics, according to the respective numbers of base pairs in the particular state. The relaxation to equilibrium of the whole system is then a superposition of different Debye processes. For a [RNA]:[SPD] ratio of 1:10, we find that the best fit of the complex kinetic behavior is described by distributions of populations for conformations A and B that peak at $\Delta bp = 6$ and $\Delta bp = 5$, respectively (Figure 5, panel e). In other words, we find that conformations with only five base pairs would be the most populated conformers during the refolding. This number of conformations with five base pairs corresponds to the maximum number of base pairs that ground-state conformers A and B can form simultaneously in a single RNA chain and that are therefore mutually nonexclusive. From these theoretical considerations, we obtain a structure of two times five nonexcluding base pairs. In order to evaluate whether these 10 base pairs could be formed, we modeled this arrangement of base pairs by the use of a coarse-grained model implemented in NAST

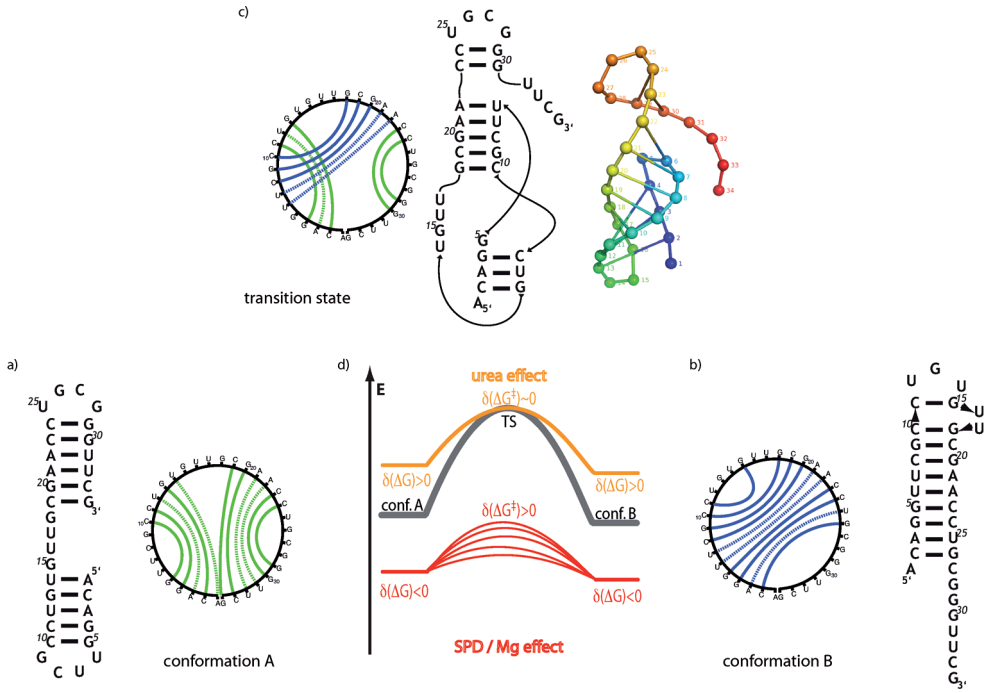

Figure 6. Representation of the main conformers of the folding trajectory of the bistable 34mer RNA and their positions along the reaction coordinate. a,b) Secondary structures of conformations A and B. c) Ribbon-ball model is a coarse grained model in 3D space of the depicted secondary structure that represents the transition state on the refolding path of the RNA. The pseudoknot structure is formed by the nonexcluding base pairs of the ground-state conformations and their number accords to the number of base pairs deduced from the analysis of the kinetics. d) Schematic representation of the cosolvent effects on the energetics of the bistable system as deduced from our data, urea (yellow) destabilizes the ground states and thereby accelerates RNA refolding, while Mg^{2+} and spermidine (red) accelerate RNA folding by stabilizing the transition state that is depicted in panel c.

(*39, 40*). As shown in Figure 6, panel c, a pseudoknot structure can be adopted by the 34mer RNA sequence. Our proposal of a transition state resembling a pseudoknot for the 34mer RNA is supported by earlier investigations for a smaller bistable RNA (*29*) and the experimental finding that RNA pseudoknot structures have a higher affinity to charged cosolvents than extended structures. The pronounced affect of spermidine might come about by its high charge and the exact matching of the position of those charges for stabilizing the phosphate backbone in a pseudoknot structure (the closest PP distance in the transition state model is predicted to be 4.4 Å; the distance between positively charged nitrogens in spermidine vary between 3.4, 3.7, and 6.4 Å in the structure (PDB code 1U8D) of the guanine-sensing riboswitch).

For a number of different systems, the effects of cosolvents on RNA folding have been investigated. The tetrahymena ribozyme (*26*) and the four-way junction ribozyme (*41*) show a decrease in their folding rates when polyamines are added, presumably due to the condensing effect the polyamines. This effect might stabilize compact off-pathway intermediates of the large ribozymes and thereby slow down the rate of productive RNA folding. In contrast, for the 34mer RNA the most compact state is the on-pathway pseudoknot-like transition state and therefore the folding kinetics are accelerated. An increase of RNA folding at nondenaturing urea concentration is commonly observed, *e.g.*, for hepatitis delta virus ribozyme (*42, 43*), where it has a similar effect as rate-increasing mutations (*44*). Previous arguments that urea facilitates the partial unfolding of folding traps (*26*) is in line with our findings where the increase of the folding reaction in the 34mer system is linked to a destabilization of the ground-state conformations. The urea effect is therefore succinctly different from the mechanism observed for spermidine and Mg^{2+}.

In summary, we show that the RNA refolding kinetics are strongly dependent on the solvent conditions and increase to different extents upon addition of urea, Mg^{2+}, or spermidine. The experimentally observed kinetics of RNA refolding reactions can best be described by a model that takes the distribution of ground-state conformations into account. In the absence of cosolvents, the ground-state conformations are homogeneous, whereas addition of cosolvents destabilizes the base pairing interactions in the ground-state structures directly. Because of the strong dependence of RNA refolding on the number of base pairs, open conformations with decreased numbers of base pairs have significantly faster

refolding kinetics, and addition of cosolvents therefore leads to complex, non-monoexponential refolding kinetics. Beside destabilization of fully base-paired ground-state conformations, the cosolvents Mg^{2+} and spermidine increase the refolding rate by stabilizing a pseudoknot-like transition state through shielding the negative phosphate. It is tempting to speculate that pseudoknot structure are common models for transition states of refolding of bistable RNAs due to their ability to stabilize alternative RNA structures.

METHODS

Chemical Synthesis. Nucleotides with a photolabile protecting group were prepared as suitable building blocks for solid-phase RNA synthesis as described earlier (*29*). With a coupling yield of >98%, the incorporation of the modified building blocks into RNA sequences occurred efficiently and without side-reactions under the standard coupling and deprotection conditions, developed for the assembly of RNA sequences from 2′-*O*-TOM protected building blocks (*45*).

Real-Time NMR Experiments and Kinetic Analysis. All kinetic NMR experiments were conducted on a Bruker 800 MHz NMR spectrometer equipped with a cryogenic *z*-gradient HCN probe. To photochemically initiate the reaction, the laser setup was synchronized with the spectrometer *via* a TTL connection. The kinetic traces were recorded in a pseudo 3D data set (as previously described (*5, 29*)). Per kinetic trace, two transients were averaged. Processing and analysis of the experimental data was performed using the software FELIX (Accelrys). Nonlinear fitting of the kinetic traces was performed using Mathematica 5. The kinetic analysis was performed on the imino-peaks of the RNA, as they are sensitive reporters on the presence of a certain base pair. The traces were obtained by integrating the half-width of each peak separately over time. For fitting purposes the peaks were normalized such that each pair of imino-protons added up to unity. Fitting was conducted for each observable and resolvable imino signal. Signals from a certain conformation all reveal identical kinetic rates within experimental error .

In the absence of cosolvents, the refolding reaction follows a reversible two-state process that can be described by

$$\frac{dA}{dt} = -k_{(A\rightarrow B)}A[t] + k_{(B\rightarrow A)}B[t]$$

and

$$\frac{dB}{dt} = +k_{(A\rightarrow B)}A[t] - k_{(B\rightarrow A)}B[t]$$

where $A[t = 0] = 1$ and $B[t = 0] = 0$, resulting in eq 2a and eq 2b in integrated forms:

$$A[t] = \frac{e^{(-k_{(A\rightarrow B)}-k_{(B\rightarrow A)})t}k_{(A\rightarrow B)} + k_{(B\rightarrow A)}}{k_{(A\rightarrow B)} + k_{(B\rightarrow A)}} \quad (2a)$$

$$B[t] = -\frac{(-1 + e^{(-k_{(A\rightarrow B)}-k_{(B\rightarrow A)})t})k_{(A\rightarrow B)}}{k_{(A\rightarrow B)} + k_{(B\rightarrow A)}} \quad (2b)$$

The quantitative kinetic analyses applied in the presence of Mg^{2+} and spermidine are described in the main text eq 1, for the qualitative description we used a modification of formulas 2 by introducing a stretch factor *b*:

$$A[t] = \frac{e^{(-k_{(A\rightarrow B)}-k_{(B\rightarrow A)})t^b}k_{(A\rightarrow B)} + k_{(B\rightarrow A)}}{k_{(A\rightarrow B)} + k_{(B\rightarrow A)}} \quad (3a)$$

and

$$B[t] = -\frac{(-1 + e^{(-k_{(A\rightarrow B)}-k_{(B\rightarrow A)})t^b})k_{(A\rightarrow B)}}{k_{(A\rightarrow B)} + k_{(B\rightarrow A)}} \quad (3b)$$

NMR Spectroscopy. Spectra were measured at temperatures between 283 and 313 K at a Bruker 800 MHz spectrometer equipped with a cryogenic *z*-gradient HCN probe. The water suppression was achieved by application of jump-return (*46*) pulse trains. ^{1}H pulses were applied on resonance of the water frequency with field strength of 29.4 kHz. Sufficient S/N was achieved by recording a single transient at 0.1 mM RNA samples. For static measurements, 128 transients were averaged, the relaxation delay was set to 1.2 s, and the spectral width was 25 ppm. For the assignment of imino-proton resonances, jump-return NOESY spectra were recorded at 278 K in 9:1 H_2O/D_2O, 25 mM potassium phosphate buffer containing 50 mM NaCl, pH 6.5. Hard power pulses were applied at the midpoint of all RNA ^{1}H resonances prior to the mixing time and at the water frequency subsequent to the mixing time. The spectra were recorded with spectral widths of 13 and 25 ppm for the indirect and direct dimensions, and 1024 and 4096 points were recorded for t_1 and t_2, respectively. Gradients had a SINE shape and were applied with a strength of 44 G cm^{-1}. The relaxation delay was 2 s; the mixing time ranged between 150 and 250 ms. Other ^{1}H resonances were assigned by recording soft-watergate NOESY spectra that were applied with similar parameters.

CD Spectroscopy. All spectra were recorded on a CD-spectrometer J-810 (JASCO) in a thermostatic cuvette holder. Samples were placed in quartz cuvettes with a pathway length of 0.1 cm and a sample volume of 250 μL. Static spectra were recorded at a temperature of 293 K, and baseline correction was applied by subtracting a spectrum recorded on plain buffer solution. The acquisition parameters were set to a wavelength range of 350 to 200 nm, a scanning speed of 100 nm min^{-1} and a bandwidth of 1 nm. Displayed spectra were recorded with 4 scans each.

Acknowledgment: We thank J. Buck for insightful discussions and R. Schroeder for insightful discussions and support. The work was financially supported by the DFG (SFB 579 "RNA-Ligand-Wechselwirkungen"), the "Studienstiftung des Deutschen Volkes" (B.F.) and the Fonds der Chemischen Industrie (H.S.). The solid-phase synthesis of the RNA molecules was carried out in Lausanne, and all NMR measurements and analysis were conducted at the Center for Biomolecular Magnetic Resonance (BMRZ) Frankfurt. H.S. is member of the DFG-funded Cluster of Excellence: Macromolecular Complexes.

Supporting Information Available: This material is available free of charge *via* the Internet at http://pubs.acs.org.

REFERENCES

1. Zarrinkar, P. P., and Williamson, J. R. (1994) Kinetic intermediates in RNA folding, *Science 265*, 918–924.
2. Schwalbe, H., Buck, J., Furtig, B., Noeske, J., and Wohnert, J. (2007) Structures of RNA switches: insight into molecular recognition and tertiary structure, *Angew. Chem., Int. Ed. 46*, 1212–1219.
3. Wong, T. N., Sosnick, T. R., and Pan, T. (2007) Folding of noncoding RNAs during transcription facilitated by pausing-induced nonnative structures, *Proc. Natl. Acad. Sci. U.S.A. 104*, 17995–18000.
4. Rajkowitsch, L., and Schroeder, R. (2007) Dissecting RNA chaperone activity, *RNA 13*, 2053–2060.
5. Furtig, B., Buck, J., Manoharan, V., Bermel, W., Jaschke, A., Wenter, P., Pitsch, S., and Schwalbe, H. (2007) Time-resolved NMR studies of RNA folding, *Biopolymers 86*, 360–383.
6. Leontis, N. B., and Westhof, E. (2003) Analysis of RNA motifs, *Curr. Opin. Struct. Biol. 13*, 300–308.
7. Westhof, E., and Fritsch, V. (2000) RNA folding: beyond Watson-Crick pairs, *Structure 8*, R55–65.
8. Misra, V. K., and Draper, D. E. (1998) On the role of magnesium ions in RNA stability, *Biopolymers 48*, 113–135.
9. Bai, Y., Greenfeld, M., Travers, K. J., Chu, V. B., Lipfert, J., Doniach, S., and Herschlag, D. (2007) Quantitative and comprehensive decomposition of the ion atmosphere around nucleic acids, *J. Am. Chem. Soc. 129*, 14981–14988.
10. Bloomfield, V. A., Crothers, D. M., Tinoco, I. (2000) *Nucleic Acids: Structures, Properties and Functions*, University Science Books, Sausalito.
11. Heilman-Miller, S. L., Thirumalai, D., and Woodson, S. A. (2001) Role of counterion condensation in folding of the *Tetrahymena* ribozyme. I. Equilibrium stabilization by cations, *J. Mol. Biol. 306*, 1157–1166.
12. Bloomfield, V. A. (1997) DNA condensation by multivalent cations, *Biopolymers 44*, 269–282.
13. Porschke, D. (1984) Dynamics of DNA condensation, *Biochemistry 23*, 4821–4828.
14. Cate, J. H., Gooding, A. R., Podell, E., Zhou, K., Golden, B. L., Kundrot, C. E., Cech, T. R., and Doudna, J. A. (1996) Crystal structure of a group I ribozyme domain: principles of RNA packing, *Science 273*, 1678–1685.
15. Cole, P. E., Yang, S. K., and Crothers, D. M. (1972) Conformational changes of transfer ribonucleic acid. Equilibrium phase diagrams, *Biochemistry 11*, 4358–4368.
16. Pyle, A. M. (1993) Ribozymes: a distinct class of metalloenzymes, *Science 261*, 709–714.
17. Anderson, J. W., Jirsch, J. D., and Fedida, D. (1995) Cation regulation of anion current activated by cell swelling in two types of human epithelial cancer cells, *J. Physiol. 483*, (Pt 3), 549–557.
18. Manning, G. S. (1978) The molecular theory of polyelectrolyte solutions with applications to the electrostatic properties of polynucleotides, *Q. Rev. Biophys. 11*, 179–246.
19. Tabor, C. W., and Tabor, H. (1984) Polyamines, *Ann. Rev. Biochem. 53*, 749–790.
20. Rubin, R. L. (1977) Spermidine-deoxyribonucleic acid interaction *in vitro* and in *Escherichia coli*, *J. Bacteriol. 129*, 916–925.
21. Williams, L. J., Barnett, G. R., Ristow, J. L., Pitkin, J., Perriere, M., and Davis, R. H. (1992) Ornithine decarboxylase gene of *Neurospora crassa*: isolation, sequence, and polyamine-mediated regulation of its mRNA, *Mol. Cell. Biol. 12*, 347–359.
22. Kusama-Eguchi, K., Watanabe, S., Irisawa, M., Watanabe, K., and Igarashi, K. (1991) Correlation between spermine stimulation of rat liver Ile-tRNA formation and structural change of the acceptor stem by spermine, *Biochem. Biophys. Res. Commun. 177*, 745–750.
23. Veress, I., Haghighi, S., Pulkka, A., and Pajunen, A. (2000) Changes in gene expression in response to polyamine depletion indicates selective stabilization of mRNAs, *Biochem. J. 346*, (Pt 1), 185–191.
24. Davis, R. H., Morris, D. R., and Coffino, P. (1992) Sequestered end products and enzyme regulation: the case of ornithine decarboxylase, *Microbiol. Rev. 56*, 280–290.
25. Watanabe, S., Kusama-Eguchi, K., Kobayashi, H., and Igarashi, K. (1991) Estimation of polyamine binding to macromolecules and ATP in bovine lymphocytes and rat liver, *J. Biol. Chem. 266*, 20803–20809.
26. Heilman-Miller, S. L., Pan, J., Thirumalai, D., and Woodson, S. A. (2001) Role of counterion condensation in folding of the *Tetrahymena* ribozyme. II. Counterion-dependence of folding kinetics, *J. Mol. Biol. 309*, 57–68.
27. Micura, R., and Hobartner, C. (2003) On secondary structure rearrangements and equilibria of small RNAs, *ChemBioChem 4*, 984–990.
28. Furtig, B., Wenter, P., Reymond, L., Richter, C., Pitsch, S., and Schwalbe, H. (2007) Conformational dynamics of bistable RNAs studied by time-resolved NMR spectroscopy, *J. Am. Chem. Soc. 129*, 16222–16229.
29. Wenter, P., Furtig, B., Hainard, A., Schwalbe, H., and Pitsch, S. (2005) Kinetics of photoinduced RNA refolding by real-time NMR spectroscopy, *Angew. Chem., Int. Ed. 44*, 2600–2603.
30. Wenter, P., Furtig, B., Hainard, A., Schwalbe, H., and Pitsch, S. (2006) A caged uridine for the selective preparation of an RNA fold and determination of its refolding kinetics by real-time NMR, *ChemBioChem 7*, 417–420.
31. Wirmer, J., Kuhn, J., and Schwalbe, H. (2001) Millisecond time resolved photo-CIDNP NMR reveals a non-native folding intermediate on the ion-induced refolding pathway of bovine alpha-lactalbumin, *Angew. Chem., Int. Ed. 40*, 4248–4251.
32. Kuhn, T., and Schwalbe, H. (2000) Monitoring the kinetics of ion-dependent protein folding by time-resolved NMR spectroscopy at atomic resolution, *J. Am. Chem. Soc. 122*, 6169–6174.
33. Kohlrausch, R. (1854) Theorie des elektrischen Rückstandes in der Leidner Flasche, *Poggendorff 91*, (56–82), 179–213.
34. Allen, F. S., Gray, D. M., and Ratliff, R. L. (1984) On the first-neighbor analysis of nucleic acid CD spectra: the definitive T-matrix and considerations of various methods, *Biopolymers 23*, 2639–2659.
35. Riazance, J. H., Baase, W. A., Johnson, W. C., Hall, K., Cruz, P., and Tinoco, I. (1985) Evidence for Z-form RNA by vacuum UV circular-dichroism, *Nucleic Acids Res. 13*, 4983–4989.
36. Gueron, M., and Leroy, J. L. (1995) Studies of base pair kinetics by NMR measurement of proton exchange, *Methods Enzymol. 261*, 383–413.
37. Laing, L. G., Gluick, T. C., and Draper, D. E. (1994) Stabilization of RNA structure by Mg ions - specific and nonspecific effects, *J. Mol. Biol. 237*, 577–587.
38. Wyatt, J. R., Puglisi, J. D., and Tinoco, I. (1990) RNA pseudoknots - stability and loop size requirements, *J. Mol. Biol. 214*, 455–470.
39. Jonikas, M. A., Radmer, R. J., and Altman, R. B. (2009) Knowledge-based instantiation of full atomic detail into coarse-grain RNA 3D structural models, *Bioinformatics 25*, 3259–3266.
40. Jonikas, M. A., Radmer, R. J., Laederach, A., Das, R., Pearlman, S., Herschlag, D., and Altman, R. B. (2009) Coarse-grained modeling of large RNA molecules with knowledge-based potentials and structural filters, *RNA 15*, 189–199.
41. Walter, F., Murchie, A. I., Thomson, J. B., and Lilley, D. M. (1998) Structure and activity of the hairpin ribozyme in its natural junction conformation: effect of metal ions, *Biochemistry 37*, 14195–14203.
42. Chadalavada, D. M., Senchak, S. E., and Bevilacqua, P. C. (2002) The folding pathway of the genomic hepatitis delta virus ribozyme is dominated by slow folding of the pseudoknots, *J. Mol. Biol. 317*, 559–575.

43. Shcherbakova, I., and Brenowitz, M. (2005) Perturbation of the hierarchical folding of a large RNA by the destabilization of its scaffold's tertiary structure, *J. Mol. Biol. 354*, 483–496.
44. Rook, M. S., Treiber, D. K., and Williamson, J. R. (1998) Fast folding mutants of the *Tetrahymena* group I ribozyme reveal a rugged folding energy landscape, *J. Mol. Biol. 281*, 609–620.
45. Wenter, P., Reymond, L., Auweter, S. D., Allain, F. H. T., and Pitsch, S. (2006) Short, synthetic and selectively C-13-labeled RNA sequences for the NMR structure determination of protein-RNA complexes, *Nucleic Acids Res.* 34.
46. Sklenar, V., and Bax, A. (1987) A new water suppression technique for generating pure-phase spectra with equal excitation over a wide bandwidth, *J. Magn. Reson. 75*, 378–383.